2004 Computational Chemistry & Materials Science Summer Institute

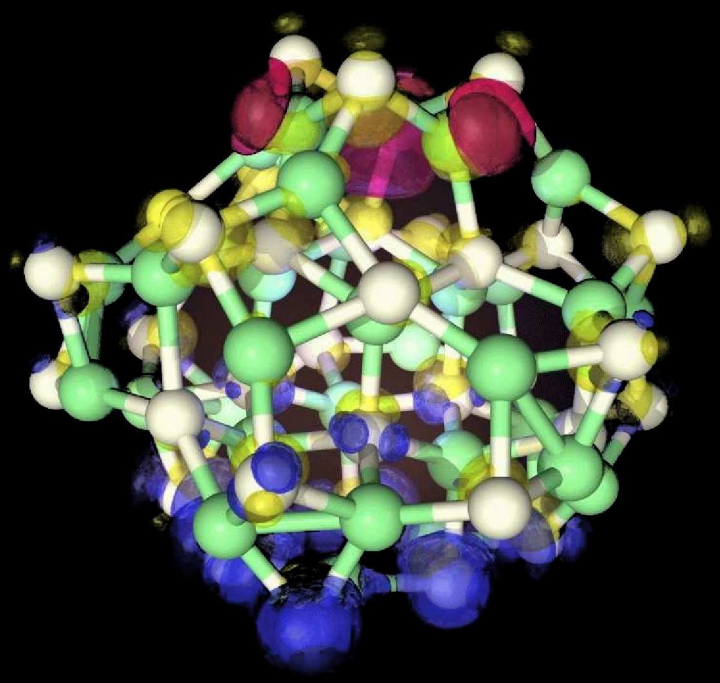

Lawrence Livermore National Laboratory
June 9–August 17, 2004

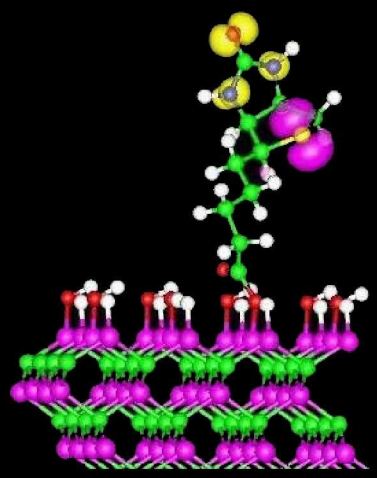

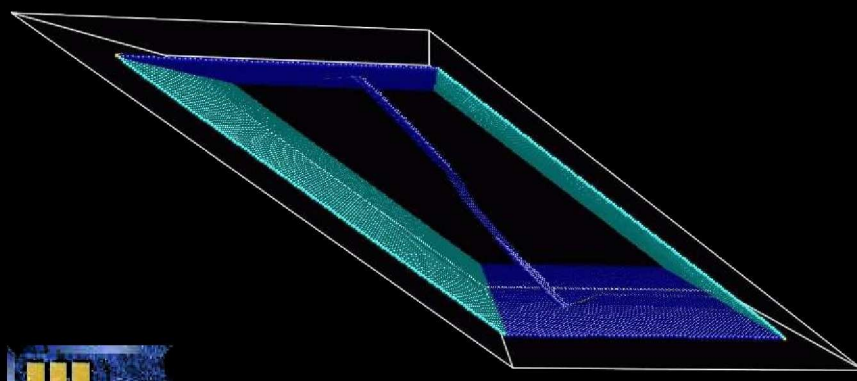

UCRL–TR–207915

About the Cover

The graphics shown on the cover were produced by the students as part of the 2004 Computational Chemistry and Materials Science (CCMS) Summer Institute program. The image at the top shows a snapshot from a simulation of a 1.5 nm wurtzite structure CdSe quantum dot. The blue, red and yellow isosurfaces contain 50% of the charge in the HOMO, LUMO and surface trap states respectively (courtesy of V. Lordi and A. Williamson). The image at the bottom left shows the HOMO states of a biotin molecule attached to a silicon-carbide (001) surface (courtesy of Y. Kanai and G. Cicero). The image at the bottom right shows a mixed character dislocation in molybdenum as it reacts to the image stresses due to the free surface (courtesy Z. Yang and M. Tang). The images on the back cover resulted from a Coupled Atomistic Dislocation Dynamics (CADD) simulation of dislocations impinging and interacting with a grain (twin) boundary in aluminum (courtesy of M. Dewald and R. Rudd). Each of these images was produced in a computer simulation conducted as part of a student project during the 2004 CCMS Summer Institute.

About this Publication - UCRL-TR-207915

This document has been prepared as an account of work sponsored by an agency of the United States Government of the 2004 Lawrence Livermore National Laboratory Computational Chemistry and Materials Science Summer Institute. This work was performed under the auspices of the U.S. Department of Energy by the University of California, Lawrence Livermore National Laboratory, under Contract No. W-7405-Eng-48. Please address any correspondence to LLNL CCMS Summer Institute, Mail Stop L-268, Lawrence Livermore National Laboratory, P.O. Box 808, Livermore CA 94551 USA. Our e-mail address is summer.institute@llnl.gov.

Disclaimer

This document was prepared as an account of work sponsored by an agency of the United States Government. Neither the United States Government nor the University of California nor any of their employees makes any warranty, express or implied, or assumes any legal liability or responsibility for the accuracy, completeness or usefulness of any information, apparatus, product, process disclosed, or represents that its use would not infringe privately owned rights. Reference herein to any specific commercial product, process or service by trade name, trademark, manufacturer or otherwise, does not necessarily constitute or imply its endorsement, recommendation or favoring by the United States Government or the University of California. The views and opinions of authors expressed herein do not necessarily state or reflect those of the United States Government or the University of California, and shall not be used for advertising or product endorsement purposes.

© 2004. The Regents of the University of California. All rights reserved. This document has been authored by the Regents of the University of California under Contract W-7405-Eng-48 with the U.S. Government. To request permission to use any material contained in this document, please submit your request in writing to the Business Services Department, Information Management Group, Lawrence Livermore National Laboratory, Mail Stop L-664, P.O. Box 808, Livermore CA 94551 USA, or e-mail the request to report-orders@llnl.gov.

2004 LLNL Computational Chemistry and Materials Science Summer Institute

June 9 – August 17, 2004

Lawrence Livermore National Laboratory
7000 East Avenue, L-268
Livermore, CA 94550 USA

Web site: http://www-cms.llnl.gov/ccms_summer_inst/

Director: Dr. Michael McElfresh
Academic Director: Dr. Robert E. Rudd
Summer Institute Coordinator: Ms. Jody Reyes-Quick

Organizing Committee:
Dr. Vasily Bulatov
Dr. Christian Mailhiot
Dr. Carl Melius
Dr. James Stolken
Dr. Andrew Williamson

Sponsors:
LLNL Chemistry & Materials Sci.
LLNL Defense & Nuclear Tech.
LLNL Director's Office
LLNL Engineering
LLNL Physics & Advanced Tech.

CCMS Summer Institute

The Lawrence Livermore National Laboratory (LLNL) Computational Chemistry and Materials Science (CCMS) Summer Institute is a program that allows graduate students to visit LLNL for ten weeks during the summer for an extraordinary educational experience in the computational sciences. Each student conducts research supervised by an LLNL staff member, attends lectures on some of the most exciting current developments in computational science, takes tours of LLNL facilities such as NIF and Power Wall in the Center for Advanced Scientific Computing (CASC), and participates in informal interactions with the other students and LLNL staff. This year the program ran from June 9 to August 17, with eleven graduate students participating from premiere university programs around the world.

The research that the students conducted ranged from the simulation of materials under extreme conditions to computational biology to nanoscience. For example, research topics included shock-induced melting, dislocation properties related to material strength, bond additivity in quantum chemistry, and optical properties of quantum dots. On August 12 the students each made a poster presentation of his or her project in the lab-wide poster symposium held at the new LLNL Central Cafe. The posters are included below. You will also find a table listing the students and their affiliation, local host, home organization and project name.

The students also attended a lecture program including 13 mini-courses presented by recognized leaders in the areas of computational physics, chemistry, materials science, and engineering. In all, 20 hours of lectures were given. The lecturers came from both within and outside LLNL, chosen based on both the expertise in research and their ability to give interesting, pedagogical lectures. The courses were again held primarily in the new auditorium in Building 155 of LLNL. The courses were advertised throughout LLNL, as well as at Sandia National Laboratories and local universities including UC-Berkeley, UC-Davis, and Stanford. This year the mini-courses focused on the nanoscience of materials and biological systems as well as a number of advanced computational techniques.

One goal of the CCMS Summer Institute program is to raise the visibility of the cutting edge computational research at LLNL among the graduate student communities at universities. Many of the students who participate in the CCMS Summer Institute arrive without any knowledge of the research conducted at LLNL. During their stay, the students are exposed to some of the outstanding research conducted at LLNL, and in some cases even come to consider a national lab as an attractive career option. As examples, one of the students from the 2001 Summer Institute program, Leonard Harris, decided to stay at LLNL to complete his dissertation, one of the students, Matthew Busche, from the 2001 Summer Institute has recently been hired as a staff member in NTED and one of the students, Giancarlo Cicero, from the 2003 Summer Institute program has been hired recently as a postdoc in H Division. We know of one CCMS Summer Institute alumnus, Chaitanya Deo, who has been hired at another national laboratory. In other cases, the visit produced important papers and on-going collaborations. It is already clear that several of this year's students will continue to work with their LLNL host in some capacity.

This report provides a summary of the 2004 CCMS Summer Institute. It describes the organization, the students and hosts who participated and the mini-courses. Copies of the student posters are also included.

Acknowledgments: We would like to give special thanks to Jody Reyes-Quick who administered the program this year, to Randy Simpson and CChED who have provided the support for this program's administration.

Summer Institute Organizing Committee

2004 Organizing Committee: (left to right) Michael McElfresh (Director), Robert Rudd (Academic Director), Vasily Bulatov, Christian Mailhiot and Andrew Williamson; not pictured: Carl Melius and James Stolken

2004 Summer Institute Students

Student Name	University	LLNL Host	Thesis Advisor	LLNL Project Title
Bharthwaj Anantharaman	MIT	Carl Melius	Gregory McRae	Bond Additivity Corrections for G3 Based Quantum Chemistry Methods
Michael Dewald	Brown	Robert Rudd	William Curtin	Dislocation Pile Up/Grain Boundary Interactions
Yosuke Kanai	Princeton	Eric Schwegler	Roberto Car	Biotin Chemisorption on Clean and Hydroxylated Si-SiC(001) Surfaces
Love Koci	Uppsala	Eduardo Bringa	Rajeev Ahuja	Simulation of Shock Induced Melting of Ni using Molecular Dynamics-Two Temperature Model Coupling
Vincent Lordi	Stanford	Andrew Williamson	James Harris	Structural and Optical Properties of CdSe Quantum Dots
Cory Lowe	Lehigh Univ.	Vasily Bulatov	Jeffrey Rickman	Activated State of a Dislocation Kink-Pair Under Stress
Anna Marzegalli	Univ. Milan Bicocca	Vasily Bulatov	Leo Miglio	60 Degree Dislocation Dissociation Reaction in Heteroepitaxial Silicon: a continuum model compared with ab initio and molecular dynamics calculations

Chitral Naik	Colorado School of Mines	Bill Pitz	Anthony Dean	Detailed Chemical Kinetic Modeling of Oxidation of Surrogate Fuels for Gasoline: Application to HCCI Engine
Paul Schuck	Arizona State	Babak Sadigh	Jim Adams	A Study of Dislocation Vibrational Frequencies in BCC Molybdenum
Zhijian Yang	Princeton	Meijie Tang	Weinan E	Atomistic Simulation of Dislocation in (BCC) Thin Film
Diana Yi	UC-Berkeley	Alison Kubota	Daryl Chrzan	Nucleation and Growth Models: Kinetic Monte Carlo vs. Rate Equations

2004 Summer Schedule

June 23 11:30 a.m. B151 R1209 Room	Wavefunction methods in Quantum Chemistry	**Martin Head-Gordon**, UC Berkeley
June 23 2:00–3:30 p.m. B155 Auditorium	Time Dependent Density Functional Calculations	**Martin Head-Gordon**, UC Berkeley
June 28 2:00–3:30 p.m. B155 Auditorium	Theory and Applications of Density Functional Linear Response Theory	**Vidvuds Ozolins**, UCLA
June 30 2:00–3:30 p.m. B155 Auditorium	Theory and Applications of Density Functional Linear Response Theory	**Vidvuds Ozolins**, UCLA
July 1 2:00–3:30 p.m. B155 Auditorium	Theory and Applications of Density Functional Linear Response Theory	**Vidvuds Ozolins**, UCLA
July 12 10:30-12:00 p.m. B155 Auditorium	Statistical Models of Complex Systems	**Arup Chakraborty**, UC Berkeley
July 12 2:00-3:00 p.m. B155	Statistical Models of Biological Systems	**Arup Chakraborty**, UC Berkeley

Auditorium		
July 13 3:30–4:30 p.m. Auditorium	Computational Science at LLNL	**Steven Ashby**, LLNL/Comp
2:00–3:30 p.m. B155 Auditorium	Finite Element Modeling for Ab Initio Calculations	**John Pask**, LLNL/PAT
2:00–3:30 p.m. B155	Real-space methods for DFT calculations in O(N) operations	**Fattebert**, LLNL/Comp
2:00–3:30 p.m. B155 Auditorium	Overview of Continuum Solid Mechanics	**Tom Arsenlis**, LLNL/CMS
2:00–3:30 p.m. B155 Auditorium	Variational and Numerical Methods in Continuum Mechanics	**James Stölken**, LLNL/Eng
2:00–3:30 p.m. B155 Auditorium	Material Models of Elasticity, Plasticity and	**R. Becker**, LLNL/Eng
August 9 p.m. B155 Auditorium	Modeling of Defects in Crystals: From	**Robert V. Kukta**, niversity of New York at Stony Brook
August 10 1:00–2:00 p.m. B451 White Room	Power Wall Visualization	**Francois Gygi**, LLNL/Comp **Meijie Tang**, LLNL/PAT **Eduardo Bringa**, LLNL/CMS

		Robert Rudd, LLNL/PAT
August 10 2:00–3:30 p.m. Auditorium	Modeling of Defects in Crystals: From Atomistics to Continuum Mechanics	**Robert V. Kukta**, State University of New York at Stony Brook
2:00–3:30 p.m. B151 R1209 Stevenson Room	Equation Free Methods	**Yannis Kevrekides**, Princeton
10:30–12:00 p.m. B155 Auditorium	Part 1: Spin Injection Part 2: Electronic Transport, Hysteresis, and Switching in Molecular Nanostructures	**Bratkovsky**, Hewlett-Packard Laboratories

CCMS Summer Institute Student Posters

LLNL held a summer student research poster symposium on August 12, 2004, as a forum "to increase awareness of the student research achievements, provide models of exemplary research and facilitate student participation in the national laboratories' scientific and engineering communities." [Newsline, August 2, 2002; See also August 13, 2004] The Summer Institute students joined many other students from throughout the lab to present their research. The event was very well attended in the spacious venue of the newly constructed Central Cafe. The posters cover research that the students conducted while at LLNL, and they indicate the very high level of work that was accomplished during their ten-week stay.

The following pages present the posters in alphabetical order of the student's surname. Full-sized versions of the posters are available for viewing as well.

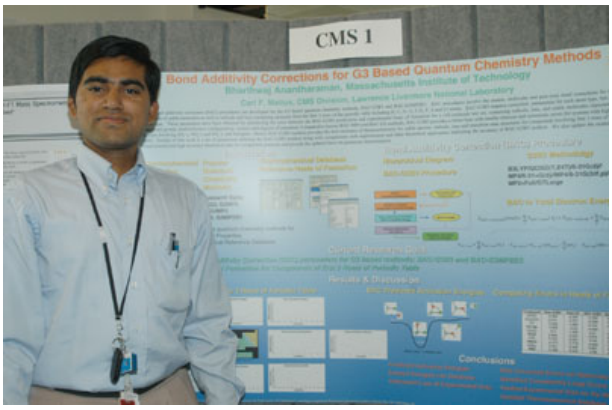

B. Anantharaman from MIT working in CMS

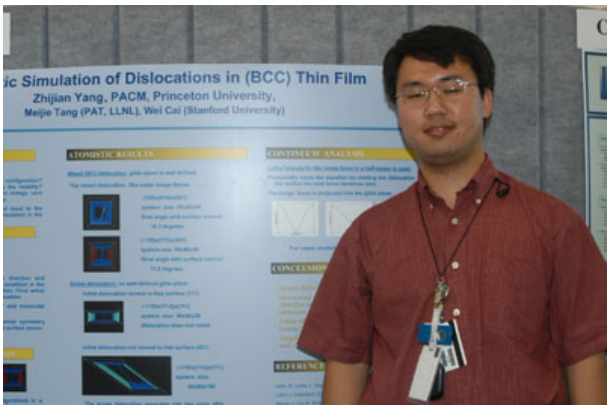

Z. Yang from Princeton working in PAT

Bond Additivity Corrections for G3 Based Quantum Chemistry Methods

Bharthwaj Anantharaman, Massachusetts Institute of Technology

Carl F. Melius, CMS Division, Lawrence Livermore National Laboratory

New bond additivity correction (BAC) procedures are developed for the G3 based quantum chemistry methods, BAC-G3B3 and BAC-G3MP2B3. BAC procedures involve the atomic, molecular and pair-wise bond corrections for the heats of formation of stable molecules as well as radicals and ions containing elements from the first 3 rows of the periodic table including H, C, N, O, F,Si, P, S and Cl atoms. BAC-G3B3 requires correction parameters for each atom type, but not for each bond type. These parameters have been obtained by minimizing the error between the BAC-G3B3 predictions and experimental heats of formation for a 142-molecule test set, containing radicals, ions, and stable molecules representing various functional groups, multireference configurations, isomers and degrees of saturation. Compared to former BAC-MP4 and BAC-G2 methods, BAC-G3B3 provides a better base with smaller inherent and systematic errors for systems with highly oxidized species involving SO_x's, NO_x's and PO_x's, and halogens. Hence, BAC-G3B3 method provides the best estimates of thermochemistry for stable species, radicals, ions and transition state structures for compounds involving first 3 rows of the periodic table. Results of this work is a set of parameters defining the BAC-G3B3 method along with comparisons with experimental and other theoretical approaches indicating the accuracy of BAC-G3B3 method. We also update the existing library of experimental and high-accuracy theoretical data for comparison purposes and provide the updated basis for parameter determination.

Introduction

Thermochemical Properties

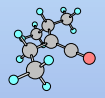

Popular Quantum Chemistry Methods

Gaussian® Suite:
G1, G2, G2MP2
G3, G3MP2
G3B3, G3MP2B3

Thermochemical Database Reference Heats of Formation

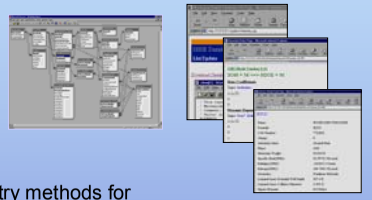

Since 1950s, efforts to correct quantum chemistry methods for
1. Accurate Thermochemical Properties
2. High Quality Thermochemical Reference Database

Bond Additivity Correction (BAC) Procedure

Hierarchical Diagram

BAC-G3B3 Procedure

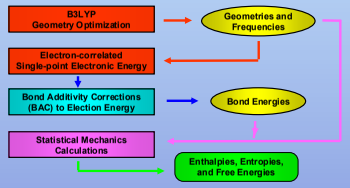

G3B3 Methodolgy

B3LYP/QCISD(T,E4T)/6-31G(d)//
MP4/6-31+G(d)//MP4/6-31G(2df,p)//
MP2=Full/GTLarge

BAC to Total Electron Energy

$$E_{BAC-correction}(total) = \sum_i E_{BAC-atom}(A_k) + E_{BAC-molecule} + \sum_{ij} E_{BAC-bond}(A_i A_j)$$

$$E_{BAC-atom} = \sum_k E_{BAC-atom}(A_k) \qquad E_{BAC-molecule} = K_{elec-pair}(spin_{molecule} - \sum_k spin_k) \qquad E_{BAC-bond}(AB) = A_{AB} e^{-dB_{AB}} + \sum_C B_{CA} + \sum_D B_{DB}$$

Current Research Goal

Develop Bond Additivity Correction (BAC) parameters for G3 based methods: BAC-G3B3 and BAC-G3MP2B3
Reference Heats of Formation for Compounds of first 3 Rows of Periodic Table

Results & Discussion

BAC Parameters for 3 Rows of Periodic Table

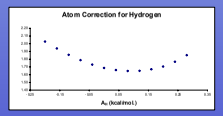

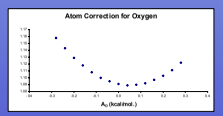

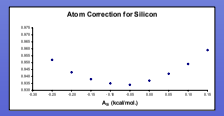

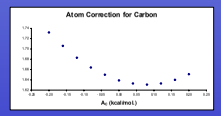

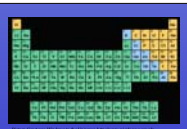

Photo Courtesy Webmeister Rich Gerstein http://www.webmeister.com/rich

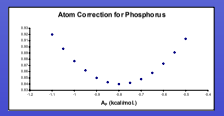

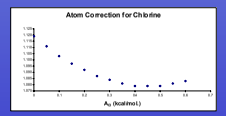

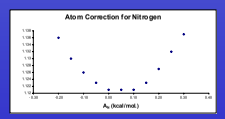

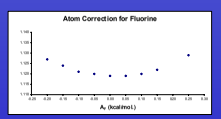

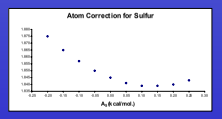

BAC Predicted Activation Energies

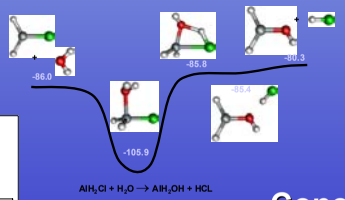

Comparing Errors in Heats of Formation

Compound	Raw-G3B3	Raw-G2	BAC-G3B3	BAC-G2
HCHO	-0.994	-2.095	-0.354	-0.767
CH_3OOH	0.531	-2.781	-0.058	0.387
CO	-0.636	-1.854	0.144	-0.714
CO 3pi	-3.926	-2.25	-4.006	-1.97
C_2H_4O	-0.4	-1.456	0.01	-0.557
CH_2S	2.944	3.222	3.574	4.029
FOF	0.723	-6.351	-0.49	-0.656
HNCO	-4.273	-4.778	-4.482	-3.868
C_2H_{10}	4.341	5.306	3.561	3.572
FNO	-5.488	-8.545	-4.88	-5.205

Conclusions

Predicted Activation Energies
Entered Energies into Database
Addressed Lack of Experimental Data

BAC Corrected Errors for Molecules
Identified Consistently Large Errors
Verified Experimental Data for the Molecules
Updated Thermochemical Database

This work was performed under the auspices of the U.S. Department of Energy by University of California Lawrence Livermore National Laboratory under contract No. W-7405-Eng-48.

UCRL-POST-205857

Dislocation Pile-up/Grain Boundary Interactions

M. Dewald[1]

R.E. Rudd[2], W.A. Curtin[1]

[1]Department of Engineering, Brown University, Providence, RI 02912

[2]PAT/H-Division, Lawrence Livermore National Laboratory, Livermore, CA 94550

A multi-scale model Coupled Atomistic Discrete Dislocation (CADD) is used to study interactions between dislocation pile-ups and grain boundaries. The physics of these interactions has both short range and long range length scales. Atomistic modeling is necessary to adequately capture the absorption and transmission phenomenon of dislocations, but because of computational limitations in pure atomistic models only small simulation cell sizes can be studied, thus not allowing any long range interaction. Continuum mechanics models long range interactions well but at present becomes inadequate at atomistic length scales. Multi-scale models, therefore, allows for the capture of phenomenon that is inherently atomistic while using large simulation cell sizes. The results using this model show that after a pile-up of 6 dislocations 1 full and 1 partial dislocation emit across the twin boundary on different slip planes.

Motivation and Goals:

Interactions between dislocation pile-ups and grain boundaries contribute to plasticity, crack initiation, and fatigue as well as other material properties. Unfortunately limited knowledge of these interactions is known. The goal of this work is to study the absorption, transmission, and damage initiation of dislocations at grain boundaries. Coupled Atomistic Discrete Dislocation (CADD), a multi-scale approach, is used to accomplish this task. This approach allows for atomistic resolution at the junction of dislocations and grain boundaries as well as large simulation sizes.

Methods:

CADD couples discrete dislocation plasticity with an atomistic model. Each coupled domain communicates across a coherent boundary, and dislocations can exist in both domains. Dislocations can seamlessly convert from one description to the other allowing each dislocation to travel unimpeded throughout the simulation cell. In this model edge dislocations are nucleated from a source in the continuum region. Each dislocation then travels to a region with a twin boundary, thus capturing the interaction. FCC aluminum was the material for this study.

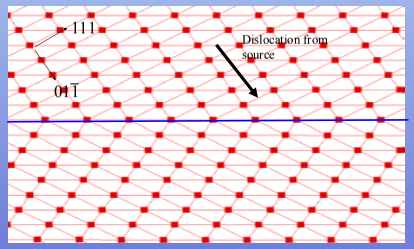

Close-up within atomistic region. The twin boundary is shown as well as the lattice directions.

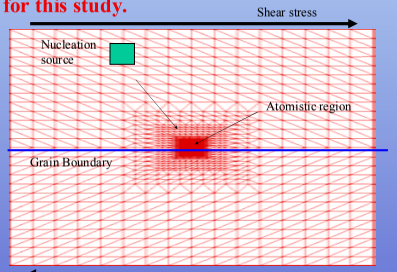

Full simulation cell is shown. The size is 1x1 microns.

Results:

The twin boundary first accommodates in coming dislocations by emitting grain boundary dislocations (GBD). The first GBD creates a step at the dislocation/twin boundary junction, while the ones emitted thereafter help to maintain the same step height at the junction. There appears to be a one-to-one correspondence between the number of partial dislocations absorbed into the boundary and the number of grain boundary dislocations emitted. After 4 partial dislocations are absorbed , 1 full dislocation and 1 partial dislocation transmit across the twin boundary on different {111} planes. The step height at the junction increases as well. This corresponds to a 6 dislocation pile-up.

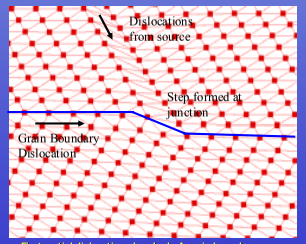

First partial dislocation absorbed. A grain boundary dislocation forms at the left which creates a step at the dislocation/twin boundary junction

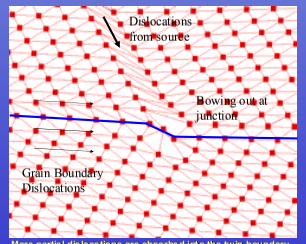

More partial dislocations are absorbed into the twin boundary, creating more grain boundary dislocations. The step height at the dislocation/twin boundary junction remains the same. Atoms bow out towards the right at the junction.

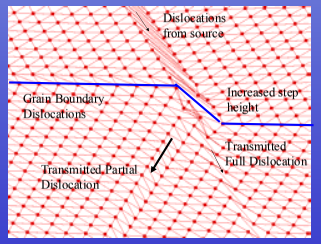

1 full dislocation and 1 partial dislocation transmitted across twin boundary. This transmission corresponds to an increase in the step height at the dislocation/twin boundary junction.

Discussion:

CADD is an effective computational model for studying the interactions between dislocation pile-ups and grain boundaries. The results posted here are the first known of this phenomenon using coupled atomistic and continuum models. Because of the vast geometric variables between different dislocations and grain boundaries, different geometries need to be studied in order to understand more clearly what are the important parameters for these interactions. CADD is capable of modeling different geometries with relative ease of implementation and can include multiple atomistic regions as well as multiple grains. For future work this would allow for the accurate study of polycrystalline materials with large number of grains within its simulation cell, thus bridging the length scales between atomistic phenomenon and microstructure.

This work was performed under the auspices of the U.S. Department of Energy by University of California Lawrence Livermore National Laboratory under contract No. W-7405-Eng-48.

UCRL xx-xxxxxxx

Biotin Chemisorption on Clean and Hydroxylated Si-SiC(001) Surfaces

Yosuke Kanai, Princeton University, NJ
Giancarlo Cicero, Giulia Galli (PAT, LLNL), Annabella Selloni, Roberto Car (Princeton Univ., NJ).

UCRL - POST - 205776

MOTIVATION

- Silicon Carbide (SiC) is a promising semiconductor material for biosensors.
  - » Biocompatibility (used for eg. artificial heart valves).
  - » Resistance to harsh environments (radiation, high T).
  - » Hydrophilic/phobic character of Si/C terminated SiC surface [1].
- Strong affinity of Biotin to Streptavidin (or Avidin) is ideal for biosensing applications.
- Chemisorption of Biotin molecule on both metal and semiconductor surfaces through esterification reaction has been recently achieved experimentally [2][3].

GOAL

Investigate the changes in structural and electronic properties of Biotin molecule and Si terminated SiC surfaces, using ab-initio calculations:

- How do binding properties of biotin to proteins (mainly related to uredo group) change upon chemisorption on Si-SiC(001) surfaces?
- How are the electronic properties of the clean and hydroxylated Si-SiC(001) surface affected by the presence of the biotin?

METHOD

- Density Functional Theory (GGA-PBE).
- Simultaneous relaxation of electronic and ionic degrees of freedom using Car-Parrinello MD.
- Non-local, *ab-initio*, norm-conserving pseudopotentials.
- Planewave expansion (80Ry cutoff) of wavefunctions.
- Supercells, with periodic boundary conditions; Vacuum along Z axis (17 Å) to avoid interaction of images. 8 layers of 16 atom/Si or C layer. Γ point.
- Calculations were carried out using the first-principles molecular dynamics GP code (F. Gygi, LLNL 1999-2003).
- PWSCF code was used for spectral analysis .

References

[1] G. Cicero, A. Catellani, and G. Galli, PRL 93, 016102 (2004).
[2] H.Morgan, D.M. Taylor and C. D'Silva, Thin Solid Films 209, 122 (1992).
[3] Didier Delabouglise, et al., Chem. Comm. 21, 2693 (2003).
[4] J. Fattebert and F. Gygi, Intl. J. Quantum Chem. 93, 139 (2003).

This work was performed under the auspices of the U.S. Department of Energy by University of California Lawrence Livermore National Laboratory under contract No. W-7405-Eng-48.

RESULTS

Biotin

Uredo group of biotin is highly polar, and it plays an important role in the hydrogen bonding to proteins (Streptavidin, Avidin).

Lowest Unoccupied Molecular Orbital (LUMO) is localized on the carboxyl group while Highest Occupied Molecular Orbital (HOMO) is highly localized on Sulfur atom and the molecular orbital right below HOMO (HOMO-1) is localized on the uredo group: most chemically reactive sites are the Sulfur atom and the carboxyl group.

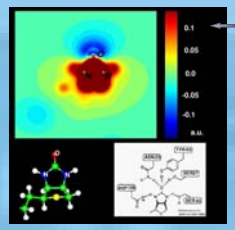

Electrostatic potential of biotin molecule around the uredo group. Oxygen as well as Nitrogen atoms are negatively charged while the Carbon atom is positively charged (Lowdin charge population analysis).

Charge density plot of selected electronic states (0.01 a.u. isosurface).

Effects of water solvation on the structural and electronic properties were assessed using a continuum solvation model [4] and found to be negligible.

Biotin on Si-SiC(001)

Si-SiC(001) surface reconstructs to form symmetric Si-Si dimers p(2x1). The clean surface has a very small band gap [E_{gap} = 0.15 eV] and is reactive. Biotin molecule chemisorbes dissociatively through the carboxyl group.

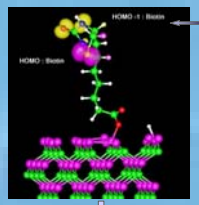

Reaction Energy: ΔE ~ -3.2 eV

OH bond of the carboxyl group dissociates forming a SiH and a SiO chemical bonds with the surface. A similar dissociation mechanism has been observed for water molecules on Si-SiC(001) surface [1]. Other Si surface dimers are affected and buckle slightly.

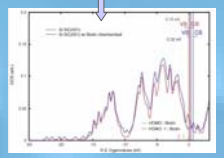

Reaction Energy: ΔE ~ -1.2 eV

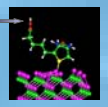

Biotin could also attach by dative bond through the sulfur atom. However, the interaction is much weaker (by 2.0 eV) than the carboxyl dissociative chemisorption.

DOS (Density of States)

The clean surface presents surface states near the band gap, corresponding to the top most Si atom layer. Upon Biotin chemisorption, the Si dimers on surface undergo minor structural transformations and the corresponding electronic states are rearranged to give a larger band gap.

Biotin on hydroxylated Si-SiC(001)

Hydroxylated Si-SiC(001) surface exhibits a network of hydrogen bonded -OH groups. Biotin chemisorbes on hydroxylated surfaces via esterification of the carboxyl group as shown below:

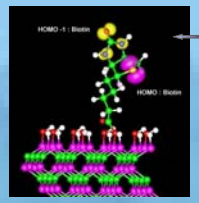

Reaction Energy: ΔE ~ 0.5 eV

The reaction is slightly endothermic. ΔE depends on the number of hydrogen bonds disrupted at surface, reducing to 0.3 eV if no hydrogen bonds are disrupted. This small value is consistent with the fact that esterification is generally an equilibrium process.

Minor structural changes of the chemisorbed biotin are observed.

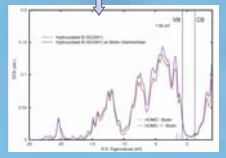

DOS (Density of States)

Band gap remains unaffected. Electronic states from the biotin are mostly superpositioned on top of the states from the hydroxylated Si-SIC(001). Projected DOS analysis reveals that states corresponding to HOMO and HOMO-1 of the biotin are well decoupled from the surface.

Summaries & Future Works

- Biotin molecule spontaneously attaches to the clean Si-SiC(001) surface. Esterification at the hydroxylated Si-SiC(001) is slighly endothermic.

  Upon Chemisorption:
- Changes in biotin structure are negligible for the both clean hydroxylated Si-SiC(001) surfaces.
- Electronic properties of the uredo group are preserved. The large spacial separation of HOMO (HOMO-1) from the carboxyl group by the alkyl chain is likely to be important.
- DOS of the hydroxylated Si-SiC(001) is essentially unchanged near the band gap while the clean Si-SiC(001) surface shows a significant rearrangement of surface electronic states.
- Work is in progress on the biotin electrostatic potential at surface, charge transfer between biotin and surface .

Activated State of a Dislocation Kink-Pair Under Stress

Cory Lowe, Lehigh University

Chemistry & Material Science, Dr. Vasily Bulatov & Dr. Wei Cai

Lawrence Livermore National Laboratory

Abstract:

The objective of this research was to calculate the activation enthalpy of a kink-pair on a screw dislocation in Tungsten as a function of applied stress. Our approach combines linear elasticity theory and the lattice "washboard" (Peierls) potential. The kink-pair geometry is considered to be a isosceles trapezoid and described using three parameters: trapezoid height h, width w, and Δ, which is a measure of the deviation from a rectangle. We wrote a Matlab code to calculate the kink-pair enthalpy as a function of these three parameters. The activation barrier for kink-pair formation is identified with the saddle point of this numerical function.The resulting stress dependence of the activated (barrier) state of the kink-pair shows several unexpected features. One of them is that, although the activation area decreases with increasing stress, as expected, the width of the kink-pair increases at the same time. Careful numerical analysis shows that the activation enthalpy exhibits unusual asymptotic behavior in the limit of stress approaching the Peierls threshold, with a fractional exponent just over 1.2. In the opposite limit of very low stress, the asymptotic behavior agrees with the classical model of Hirth-Lothe, with a fractional exponent close to 0.5.

Introduction:

The focus of this research was a detailed graph of the activation enthalpy of a kink-pair as a function of applied stress. Knowledge of the activation enthalpy allows one to calculate dislocation mobility, which impacts material properties. In particular, the yield stress of a material is directly related to dislocation mobility. Additionally, we were interested in the geometry of the kink-pair in the activated state and its stress dependence.

Kink-Pair on a Straight Screw Dislocation

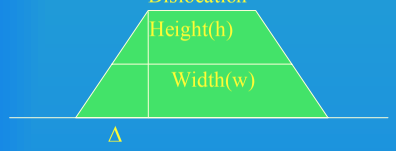

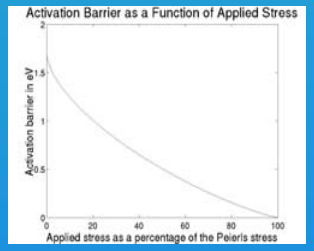

Methods:

Our first attempt to locate a saddle point for a particular applied stress relied on contour plots of the activation energy in the coordinates of kink-pair height h and width w (the third parameter, Δ, was "slaved" to h and w by way of minimization with respect to Δ for each combination of h and w). Subsequently, we modified our strategy to automate the search for the saddle-points. For that we used the complex-step derivative method to calculate, numerically, the derivatives of the enthalpy with respect to h, w, and Δ. Then, starting from the values of the three geometry parameters obtained from the contour plot, we changed applied stress in small increments and found new optimal combinations of h, w, and Δ for each value of stress.

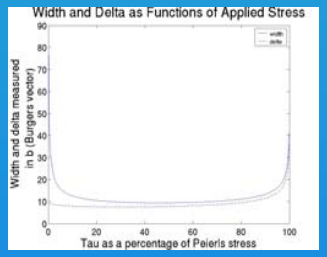

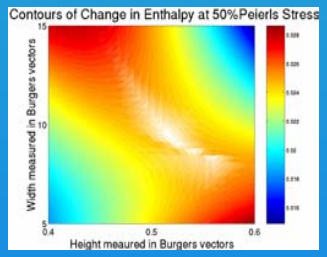

Results:

The asymptotic behavior of the activation enthalpy at low stress is well defined from kink-pair theory. In the classical model of Hirth-Lothe, $H_0 - H \propto \sqrt{\tau}$. The log-log plot below verifies that our data is in agreement with the theory in this limit. Much less is known about the high stress regime. Our data indicates that the relationship between applied stress and activation enthalpy is of the form: $H \propto (t_p - t)^{1.22}$. The one surprising result was that kink-pair width, which initially decreases with increasing stress, has a minimum and increases as the applied stress approaches the Peierls stress. This result can be seen in the graph to the right.

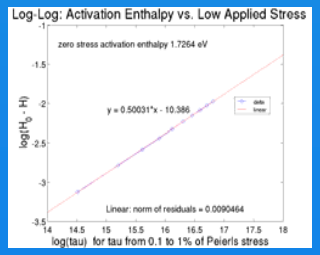

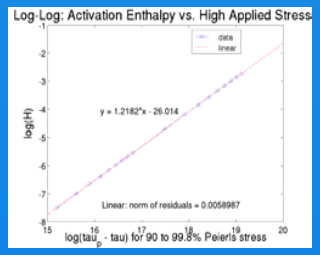

Discussion:

Further research needs to be done to check whether the high stress asymptotic behavior is universal or dependent on certain material parameters such as Poisson's ratio or the shape of the Peierls potential. Another still unexplored possibility is that the observed spreading of the activated kink-pair configuration at high stress is indicative of some soft mode vibrations of the screw dislocation.

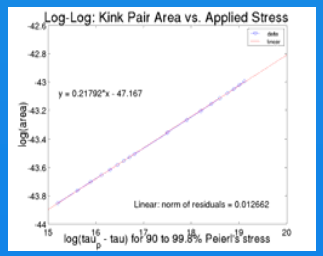

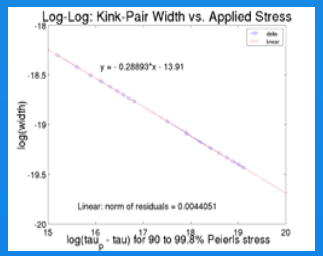

This work was performed under the auspices of the U.S. Department of Energy by University of California Lawrence Livermore National Laboratory under contract No. W-7405-Eng-48.

Detailed Chemical Kinetic Modeling of Oxidation of Surrogate Fuels for Gasoline: Application to HCCI Engine

Chitralkumar V. Naik, Colorado School of Mines, Golden, Colorado

William J. Pitz, Lawrence Livermore National Laboratory, Livermore, California

Gasoline consists of many different classes of hydrocarbons, such as paraffins, olefins, aromatics, napthenes, etc. A reaction mechanism is developed for surrogate fuels for gasoline that consist of at least one representative fuel from each of these classes. These fuels are iso-octane, n-heptane, toluene, methyl cyclohexane, and 1-pentene. The mechanism developed is based on different individual mechanisms for these fuels. Reactions important for low temperature oxidation (<1000K) and cross-reactions among different fuels are incorporated into the mechanism. The mechanism consists of 1214 species and 5401 reactions.

Single zone engine model for homogeneous charged compression ignition (HCCI) engine is used to focus on fuel chemistry effects in the engine. Experimental data are available on combustion phasing at constant intake temperature, and change in bottom dead center temperature with pressure. Three different surrogate fuel mixtures are used for the modeling. Predictions are in reasonably good agreement with these data. In addition, the heat release rate is calculated and compared to the data from experiments. The model predicted slower heat release at low temperatures than that measured. It is found that the low temperature heat release rate depends strongly on engine speeds, reactions of RO_2+HO_2, and fuel composition.

Introduction

Homogeneous charged compression ignition (HCCI) engine is emerging as a high fuel efficient engine with low NO_x emissions. The fuel is premixed and it auto-ignites in the engine due to temperature rise during the compression cycle. Because of the dominant nature of the fuel chemistry, it is very important to develop an understanding of the oxidation of fuels.

The present study is motivated by the need for a better understanding of the oxidation chemistry of gasoline. Since gasoline consists of numerous components, it is not feasible to incorporate the chemistry of all the components. Surrogate fuels to describe the behavior of gasoline are required. Ideal surrogate fuels should have all the major components present in gasoline and similar knocking behavior. In this study, we propose three surrogate mixtures.

A detailed mechanism for these surrogate fuels is developed and used for modeling the HCCI engine. It is based on detailed mechanisms for iso-octane and n-heptane developed by Curran et al., for toluene by Pitz, and for methyl cyclohexane by Curran group. Reactions important for low temperature oxidation chemistry are incorporated along with other reactions. Rate rules were developed for the set of reactions not available in the literature.

Due to the size of the mechanism, complex CFD programs cannot be used with this mechanism. A single zone well-mixed engine model as implemented in Senkin is used for the modeling with no heat losses. Heat losses in experiments are also minimized by alternate firing method*. Model predictions are in good agreement with various experimental data, such as change in combustion phasing with fueling load, change in bottom dead temperature (BDC) with pressure, as well as magnitude of heat release rate.

*Sjoberg, M. and Dec, J., SAE 2004-01-0557

Surrogate Mixtures are Created Based on Gasoline Composition, Research Octane Number (RON), Motor Octane Number (MON), and Insight from Preliminary Modeling Results

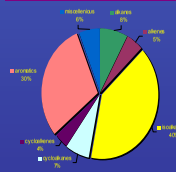

Source: http://www.mbt.kab.co.jp/product/petro/index.html

Typical composition of gasoline
Typical RON = 90.8, MON = 83.4

Surrogate Mixtures Proposed:

% Composition	Mixture-1	Mixture-2	Mixture-3
Iso-Octane	60	40	40
n-Heptane	8	10	20
Toluene	20	10	10
Methyl cyclohexane	8	40	30
1-Pentene	4	0	0
RON (linear mixing)	93.7	81.7	83.7
MON (linear mixing)	90.8	79.2	79.8
RON (blend*)	95.2	84	87.6
MON (blend*)	94.5	84.8	82

*Blend octane numbers for individual components are obtained from http://www.refiningonline.com/EngineBuilt/BI/

Mechanism Developed for Surrogate Fuels is Based on Different Mechanisms for Individual Fuels: Additional Reactions Included

- iso-Octane and n-Heptane mechanism (*Curran et al., Comb. Flame 2002, 129, 253-280*) is the starting block
- Reactions involving toluene from William J. Pitz
- Reactions involving methyl cyclohexane from the Curran group, National University of Ireland, Galway
- Some of the isomers of olefinic radicals are lumped
  - † linear hexenyl
  - † linear heptenyl
- Reactions incorporated for some of the allylic radicals with longer life times
  - † C_4H_7, C_5H_9, C_2H_3CHCHO
  - † Abstraction, disproportionation and recombination reactions considered
  - † Rate coefficients are based on Evans-Polanyi method or literature

Reactions Important for Low Temperatures are Incorporated

- At low temperatures (<1000K), alkyl peroxy radicals are in higher concentrations
- Reactions of RO_2 can be important for ignition

$$RO_2 + RH = ROOH + R\bullet \quad (1)$$

$$RO_2 + HO_2 = ROOH + O_2 \quad (2)$$

$$R'O_2 + R''O_2 = R'O\bullet + R''O\bullet + O_2 \quad (3)$$

$$ROOH = RO\bullet + OH \quad \text{(Chain branching)}$$

- Cross reactions possible between RO_2 with different R groups
- Rate coefficients for Rxn. 1 (RO_2+RH) are assigned based on abstraction by methylperoxy radical
- Generic rate coefficients used for RO_2+RO_2 reactions

Rate Rules Developed for Reactions Not Incorporated Earlier

	A	n	Ea
Abstraction by primary allylic radical from olefin			
Olefin + C_3H_7 = Alkenyl + C_3H_8	1.00E+11	0	16000
Olefin + C_3H_8 = Alkenyl + C_3H_{10}	1.00E+11	0	16000
Abstraction by secondary allylic radical from olefin			
Olefin + C_2H_3CHCHO = Alkenyl + $C_2H_3CH_2CHO$	2.86E+10	0	18000
Abstraction by benzyl radical from olefin			
Olefin + $C_6H_5CH_2$ = Alkenyl + $C_6H_5CH_3$	1.00E+11	0	17000
Abstraction by generic RO_2 radical			
RO_2 + CH_2O = ROOH + HCO	1.00E+12	0	9000
RO_2 + C_6H_5CHO = ROOH + C_6H_5C•O	3.00E+12	0	9000
RO_2 + H_2O_2 = ROOH + HO_2	1.32E+04	2.5	9560

(Rate expression is per H abstractable, cm-mol-sec-cal units)

HCCI Engine: Fuel Chemistry Dominates

- Higher fuel efficiency
  - † Lean operation
- Characteristics from SI and diesel engines: No-spark and premixed fuel
- Auto-ignition of fuel most important
- Experimental data from Sandia National Laboratories
- Single zone model with *no heat losses* used for modeling (as implemented in the IC engine feature of Senkin*)
  - † *Qualitative* description of the process expected

*Version 3.2 from Sandia Lab.

Combustion Phasing vs. Fuel Loading at Constant Temperature: Captured

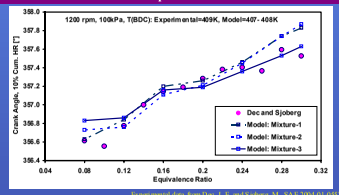

Experimental data from Dec, J. E. and Sjoberg, M., SAE 2004-01-0557

- Combustion phasing is retarded with increasing fuel loading at constant intake temperature due to:
  - † increased specific heats lowers the ratio γ ($=C_p/C_v$)
  - † compression heating is reduced

Change in BDC Temperature with Pressure Sweep: Predicted Pressure Effect is Slightly Less than that Observed

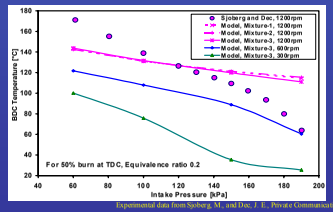

Experimental data from Sjoberg, M., and Dec, J. E., Private Communications

- Highly sensitive to engine speed
- Stronger pressure dependence at higher pressure is due to onset of the low temperature heat release (at early times before TDC)

Predicted Low Temperature Heat Release Slower than Observed : Sensitive to Speed, RO_2+HO_2 Rate Constant, and Fuel Composition

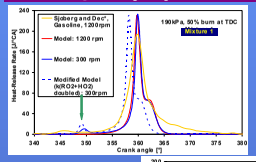

Low temperature heat release:

- Observed only at higher pressures (190kPa)
- Increases with increase in RO_2+HO_2 rate constant

- Increases at lower speeds
- Increases with the increase in the amount of n-heptane

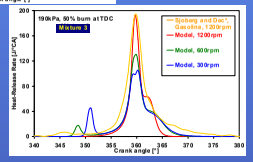

*Private Communications

Fraction of Fuel Carbon in Products CO and CO2: Captured

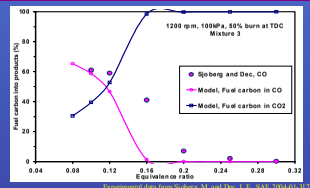

Experimental data from Sjoberg, M. and Dec, J. E., SAE 2004-01-3173

Guidelines for Future Work

- Further sensitivity analysis for low temperature heat release
- Include low temperature chemistry for methyl cyclohexane in the mechanism
- Modeling the effect of variation in engine speed
- Incorporating heat transfer in the model
- Study the effect of residues
- Reduction of the mechanism to be used in multi-zone CFD program

Acknowledgement

Authors acknowledge collaborators at Sandia National Laboratories: Magnus Sjöberg for providing the valuable experimental data on HCCI engine and scripts for modeling, and Andy Lutz for the support with Senkin software used for this work.

This work was performed under the auspices of the U.S. Department of Energy by University of California Lawrence Livermore National Laboratory under contract No. W-7405-Eng-48.

A Study of Dislocation Vibrational Frequencies in BCC Molybdenum

Paul Schuck, Arizona State University,

Chemistry and Materials Science, Babak Sadigh, Lawrence Livermore National Laboratory,

This study investigated the vibrational properties of screw dislocations in BCC Molybdenum. Vibrational frequencies were used to find unstable modes and understand dislocation movement. Two different crystal sizes of 4,800 and 48,000 atoms were investigated. When the length of the dislocation is increased, symmetry breaking in the frequency modes occur and hence a lower energy results. Dislocation length needs to be considered when performing simulations of screw dislocation movements.

Introduction:

Dislocations play an important role in the properties of materials. Much research has been completed investigating the nature of dislocation movement, but the mechanism is elusive. Analyzing the low frequency modes can provide insight into atom vibrations and unstable states that lead to dislocation movement.

Methods:

Screw dislocations are visually represented as a set of two triangular "tubes". These tubes represent an area in the crystal with high atomic distortion. See Figure 1.

To better understand dislocation movement, a shearing force is applied to the outside of the crystal. This shear is simulated by changing the cell dimensions so that the top of the crystal is moved while the base remains fixed. An angle θ represents the shift in the crystal structure. See Figure 2.

Once the crystal structure has been determined, a Finnis-Sinclair Potential is used to calculate the forces between the atoms. The vibrational frequencies are calculated by solving for the eigenvalues of the Dynamical matrix.

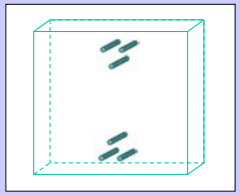

Figure 1: Two Triangular "tubes" representing a pair of screw dislocations

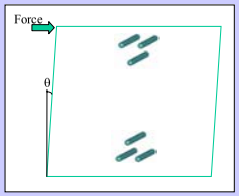

Figure 2: Representation of shearing force on crystal structure with angle θ defined

Results:

The results of the calculations are a spectrum of frequencies that exist in the crystal and are represented by a frequency density of states (DOS). For these calculations, two different crystal sizes were investigated. The first case is a 4,800 atom cell with a dislocation length of 5 atoms. The second case is a 48,000 atom cell with a dislocation length of 50 atoms. Three different angles were used (0°, 1.2°, 2.0°). Negative frequencies represent imaginary frequencies and are useful to show where unstable states exist and hence dislocation movement. Notice the trend in the DOS plots that as the angle is increased, the peaks shift to the left and more imaginary frequencies occur.

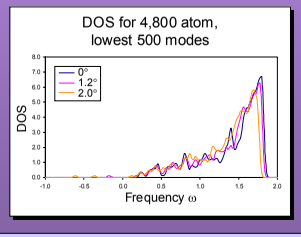

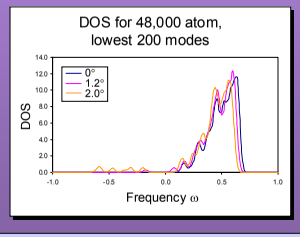

Projecting the DOS onto the dislocation atoms show which frequency modes are most significant for the dislocation. The two plots below show the projected DOS for both crystal sizes. Both sizes show a significant peak at –0.36 for 2.0°.

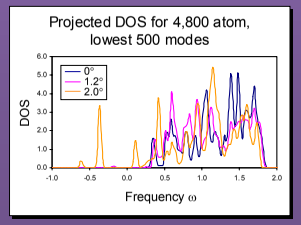

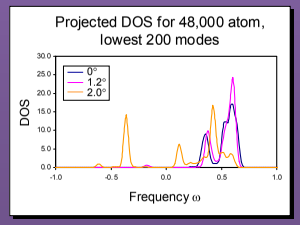

Plotting out the eigenvectors for a certain frequency mode show how the atoms vibrate. Figures 3 and 4 show a visual representation of the eigenvectors at the –0.36 frequency for the 4,800 and 48,000 atom case respectively. The teal atoms represent the original atom position while the red atoms represent the vibration direction and relative magnitude.

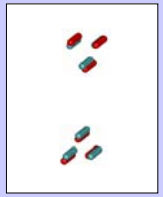

Figure 3: Visual representation of eigenvectors for 4,800 atom case

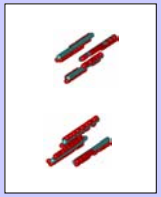

Figure 4: Visual representation of eigenvectors for 48,000 atom case

Discussion:

The 4,800 atom case looks very symmetric and the atoms all vibrate in the same phase. The 48,000 atom case is not symmetric and the atoms vibrate in different directions. These results show that the symmetry breaking occurs when the length of the dislocation is increased. Breaking the symmetry lowers the energy. Thus, a lower force is required to move the atoms for a longer dislocation. When performing simulations for screw dislocation movement, taking in account the length of the dislocation needs to be considered.

This work was performed under the auspices of the U.S. Department of Energy by University of California Lawrence Livermore National Laboratory under contract No. W-7405-Eng-48.

UCRL#

Atomistic Simulation of Dislocations in (BCC) Thin Film

Zhijian Yang, PACM, Princeton University,

Meijie Tang (PAT, LLNL), Wei Cai (Stanford University)

MOTIVATION

(BCC) Dislocation behavior in thin film:

Try to understand: what is the equilibrium configuration? how does it move under stress? what is the mobility? Focus on different energy resources: elastic energy, core energy, image force and surface step energy.

Also provide bench mark comparison and input to the larger length scale dislocation dynamics simulation in the dynamics of metals project at LLNL.

METHOD

MD++ code developed by Wei Cai et. al

Finnis-Sinclair potential for Molybdenum.

Burgers' vector always [1 1 1].

Construct free surfaces normal to one direction and dislocation dipole with periodic boundary condition in the other two directions. Remove one dislocation. Final setup has two pairs of free surfaces and one dislocation.

Conjugate gradient relaxation at zero T and molecular dynamics simulation at finite T

Visualized with energy criterion and central symmetry parameter criterion for dislocation core abd surface atoms.

AN EXAMPLE OF RELAXATION

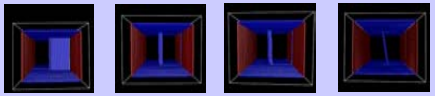

Snapshots of a sequence of atomic configurations in a typical relaxation. First, the stacking fault of atoms in the cut plane is relaxed. Second, the dislocation begins to tilt starting from two ends and propagating to the center. Finally, the equilibrium configuration is reached.

ATOMISTIC RESULTS

Mixed [001] dislocation: glide plane is well defined

The mixed dislocation tilts under image forces

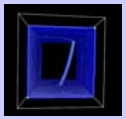

(100)x(010)x(001)

system size: 50x40x40

final angle with surface normal:

19.3 degrees

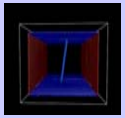

(-110)x(110)x(001)

system size: 50x40x40

filnal angle with surface normal:

11.9 degrees

Screw dislocation: no well-defined glide plane

Initial dislocation normal to free surface (111)

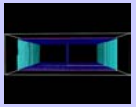

(-110)x(11-2)x(111)

system size: 50x40x20

dislocation does not rotate

Initial dislocation not normal to free surface (001)

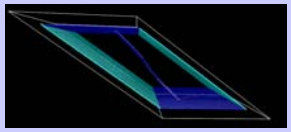

(-110)x(110)x(111)

system size:

60x60x100

The screw dislocation separates into two parts after relaxation. Each part becomes a mixed dislocation and they stay in the different glide planes. The angles with surface normals are both 47 degrees.

CONTINUUM ANALYSIS

Lothe formula for the image force in a half-space is used:

Numerically solve the equation by rotating the dislocation line so that the total force becomes zero.

The image force is projected into the glide plane.

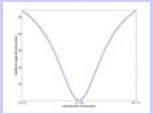

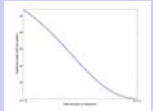

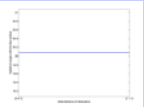

For cases studied above: b=[111], n=[001]

CONCLUSIONS

- Screw dislocation is special.
- Non-screw dislocations rotate from the initial direction within the glide plane, have ribbon core structure.
- Other effects: surface steps, finite size vs. periodic boudary condition.
- Ongoing work: applying stress on free surfaces and check the surface step energy

REFERENCES

Hirth JP, Lothe J. *Theory of dislocations* (Wiley, New York, 1982).

Lothe J, Indenbom VL, Chamrov VA. *Phys Stat Sol* ***(b)*** **111,** 671 (1982).

Marian J, Cai W, Bulatov VV. *Nature materials*, **3,** 158 (2004).

The work was performed under the auspices of the U.S. Department of Energy by the University of California Lawrence Livermore National Laboratory under contract No. W-7405-Eng-48.

UCRL-POST-205581

Nucleation and Growth Models: Kinetic Monte Carlo vs. Rate Equations

Diana O. Yi, U.C. Berkeley
Alison Kubota, MSTD
Lawrence Livermore National Laboratory

August 12, 2004

Abstract

Nucleation and growth modeling for bulk systems is explored using Kinetic Monte Carlo simulations and a Self-Consistent Mean-Field Rate Equation approach. The particular system studied involves thermal treatment of implantation of germanium ions into in a thin film of amorphous silica. Compatibility of the two models relies on choosing the same transition rates for diffusion through the matrix and for detachment from a cluster. Results for the average cluster size, cluster size distribution, monomer density and cluster density are compared, and show to be in good agreement.

Experimental Background

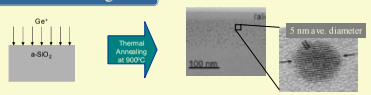

Description of Experiment

- Multi-energy (50 – 120 keV) Ge+ ions are implanted into amorphous SiO_2 (500 nm).
- Thermal treatment at 900 °C for 1 hour activates the nucleation and growth of Ge, producing a band of Ge nanocrystals as shown in (a).
- Characterization by TEM and AFM provide average nanocrystal size of 2.5 nm, with FWHM of 3.9 nm.
- TEM photograph of typical nanocrystal is shown in (b).

TEM photographs and experimental results provided by E. E. Haller and staff at Lawrence Berkeley Lab

Rate Equation Model: Derivation of Coupled Differential Equations

- What is the probability of two green atoms meeting and forming a dimer?
- What is their rate of formation?

 # atoms forming a dimer per unit time:

$$= s_1 x_1 \frac{x_1}{\left(\frac{L^3}{a^3}\right)} \frac{1}{\tau} = (s_1 a)\frac{a^2}{\tau}\left(\frac{x_1}{L^3}\right)^2 L^3$$

$$\equiv \sigma_1 \quad D \quad n_1^2 \quad L^3$$

Capture strength; # atoms; Probability of finding filled site; Rate atom moves

Coupled equations with attachment and detachment kinetics describe evolution of monomer and cluster density:

$$\frac{d\langle n_1\rangle}{dt} = -2\sigma_1 D\langle n_1\rangle^2 - D\sum_{j\geq 2}\sigma_j\langle n_1\rangle\langle n_j\rangle + 2\frac{\langle n_2\rangle}{\tau_2} + \sum_{j\geq 3}\frac{\langle n_j\rangle}{\tau_j}$$ **Monomer Density Evolution**

$$\frac{d\langle n_s\rangle}{dt} = D\sigma_{s-1}\langle n_1\rangle\langle n_{s-1}\rangle - D\sigma_s\langle n_1\rangle\langle n_s\rangle - \frac{\langle n_s\rangle}{\tau_s} + \frac{\langle n_{s+1}\rangle}{\tau_{s+1}}$$ **Cluster Density Evolution**

Rate Equation Model: Self-Consistency and Mean-Field Approximation

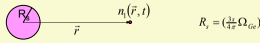

$$R_s = \left(\tfrac{3}{4\pi}\Omega_{GeO_2}\right)^{\frac{1}{3}}$$

Diffusion – Reaction Equation for n_1

$$\frac{\partial n_1}{\partial t} = D\nabla^2 n_1 - D\xi^{-2} n_1 + J$$

Mean field approximation:

$$\frac{d\langle n_1\rangle}{dt} = -D\left(2\sigma_1\langle n_1\rangle + \sum_{j\geq 2}\sigma_j\langle n_j\rangle\right)\langle n_1\rangle + \left(2\frac{\langle n_2\rangle}{\tau_2} + \sum_{j\geq 3}\frac{\langle n_j\rangle}{\tau_j}\right)$$

Assume:

$$\frac{\partial n_1}{\partial t} - \frac{dn_1}{dt} \approx 0 = \nabla^2 n_1(\vec{r}) - \xi^{-2}\left\{n_1(\vec{r}) - \langle n_1\rangle\right\}$$

Boundary Conditions provide Self-Consistency:

$$-D\left.\frac{dn_1}{dr}\right|_{R_s} = \frac{1}{4\pi R_s^2\langle n_s\rangle}\frac{d\langle n_s\rangle}{dt}$$

Self-consistent variables:

$$\sigma_s = 4\pi R_s^2\left[\frac{R_s + \xi}{a\left(e^{\gamma/s} - 1\right)(R_s + \xi) + R_s\xi}\right]$$ Capture Number

$$\xi^{-2} = 2\sigma_1\langle n_1\rangle + \sum_{j\geq 2}\sigma_j\langle n_j\rangle$$ Distance atom travels before capture

$$\tau_s^{-1} = \frac{a\sigma_{s+1}\omega_s}{4\pi R_{s+1}^2}e^{-\gamma/s}$$ Escape Rate

$$\omega_s = \frac{4\pi R_s^2}{a}Dn_\infty e^{\gamma/s}$$ Detachment Rate

where $\Gamma = \frac{2\gamma\,\Omega_{GeO_2}}{kT}$

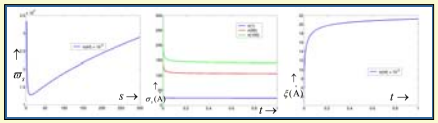

Kinetic Monte Carlo Model

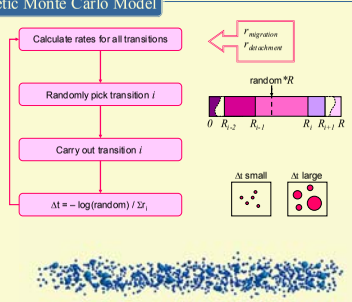

$$r_i = \begin{cases} \frac{D}{a^2} & \text{atom migration} \\ \frac{4\pi R_s^2}{a} D n_\infty e^{\gamma/R_s} & \text{atom detachment} \end{cases}$$

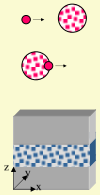

Simulation:

- Initially 1,000 atoms
- Randomly located in box
  - Everywhere in x, y
  - Band in z-direction
- Periodic Boundaries in x, y, z

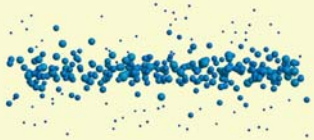

Figures rendered using Raster3D, Merritt, E.A. & Bacon, D.J. (1997) "Raster3D Photorealistic Molecular Graphics". Methods in Enzymology 277, 505-524.

Comparing Models

Parameters:

$n_{1_0} = 2.5\times 10^{-3}\,A^{-3}$ $\quad n_\infty = 10^{-6}, 10^{-8}, 10^{-10}\,A^{-3}$

$\Omega_{GeO_2} = 22.5\,A^3$ $\quad \Gamma = 8.1\,\text{Å}$

Rate of migration and detachment are the same for KMC and RE.

Rate Equations:

- Solved 1,000 coupled equations
- Used Matlab ode45 solver for 80,000 steps
- At each step, capture numbers σ_i are recalculated
- To obtain larger cluster sizes, must increase number of coupled equations

Kinetic Monte Carlo:

- Fortran KMC code
- Keep track of location and size of each particle
- Start with 20,000 atoms
- Box size of 200^3 Å^3
- Keep track of events:
  - Migration: New location of particle
  - Nucleation: Particle size increases; Particle number decreases
  - Detachment: Particle size decreases; Particle number increases

Future Plans:

- Comparison to experiment
- Include realistic energy barriers to diffusion:
  - Interstitial vs. substitutional

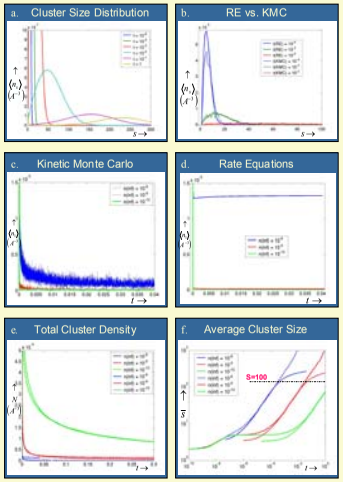

a. Cluster size distribution from RE shows a sharply peaked distribution early on, flattening over time, and with increasing size.

b. KMC and RE compared. Distribution widths compare nicely.

c. & d. Monomer density from KMC compared to RE. A higher average monomer density is found in RE for $n_\infty = 10^{-6}$ Å^{-3}.

e. Total cluster density comparison for $n_\infty = 10^{-6}$ Å^{-3} shows the same disagreement.

f. Comparing KMC and RE results for average cluster size indicates a region of agreement between s = 10 and s = 100. Below s = 10, critical cluster sizes for KMC and RE do not agree. Above s = 100, KMC clusters continue to grow while RE growth slows.

UCRL# UCRL-POST-205695

This work was performed under the auspices of the U.S. Department of Energy by University of California Lawrence Livermore National Laboratory under contract No. W-7405-Eng-48

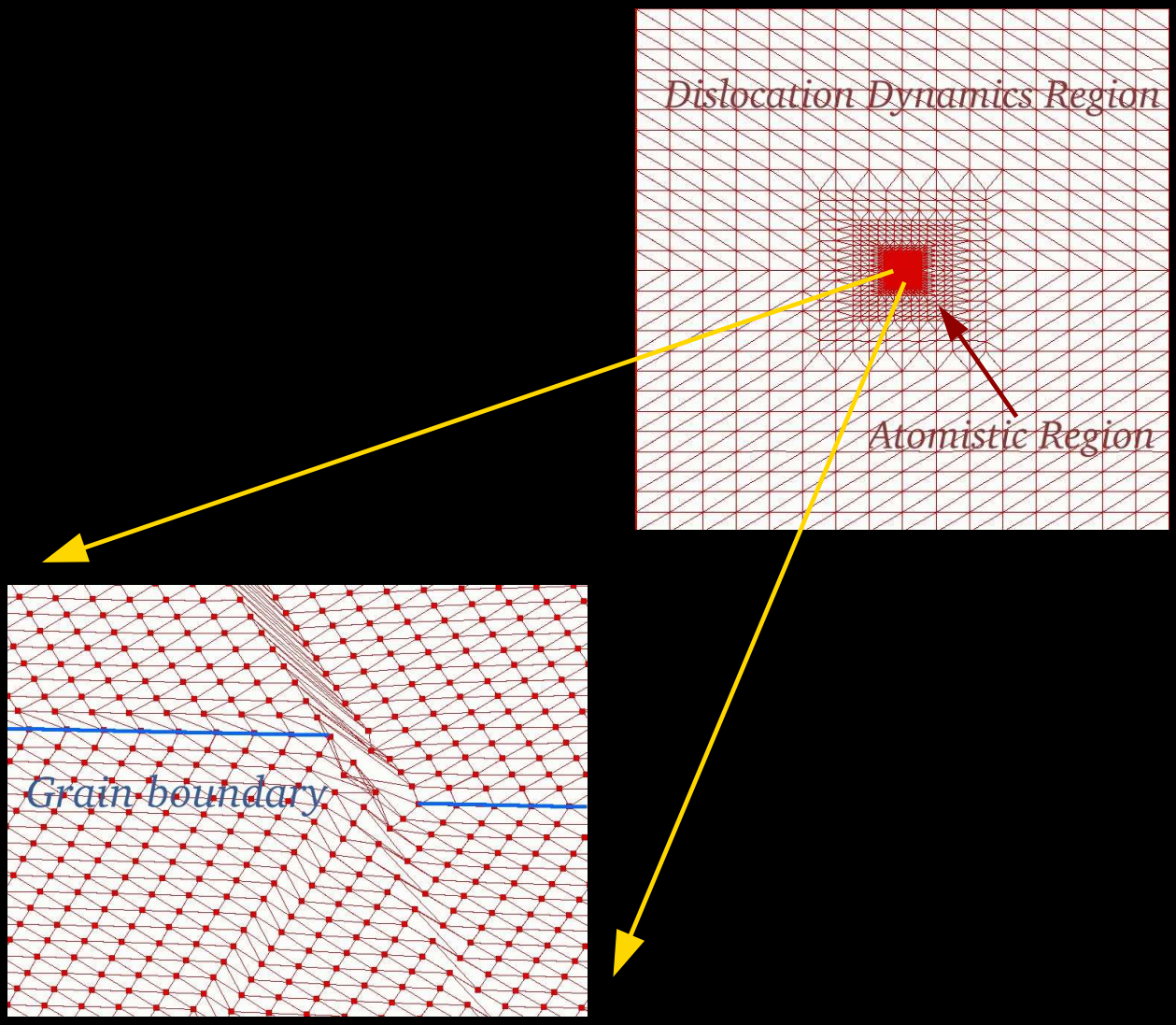

LLNL Summer Institute
on Comp. Chemistry & Materials Sci.
Lawrence Livermore National Laboratory
P.O. Box 808, Mail Stop L–268
Livermore, CA 94551 USA

Telephone: 925–422–0620 Fax: 925–422–6810
e–mail: summer.institute@llnl.gov